

Chapter 2

Laser-Plasma Accelerators

2.1 Introduction

In this chapter, the basic physics of laser-plasma accelerators (LPAs) is introduced. In the LPA, electron properties such as energy, energy distribution, bunch duration, charge and divergence depend on the interplay between the drive laser and the plasma. The first part of this chapter focuses on the basic theoretical and experimental frameworks of the drive laser. The latter part of this chapter addresses mechanisms of plasma wave excitation, electron acceleration, and electron injection in an LPA.

Section 2.2 discusses the concept of chirped pulse amplification (CPA) laser systems often used in LPA experiments. Then, the architecture of the TREX laser system, a CPA based laser, is presented. Section 2.3 introduces the theory of laser propagation in vacuum which addresses laser diffraction. Laser diffraction, if not compensated, limits the acceleration in an LPA. Then, the theory of laser guiding in a plasma waveguide to mitigate diffraction is discussed.

Section 2.4 addresses the mechanism of plasma wave excitation and its properties such as plasma wavelength, amplitude, and phase velocity. It is illustrated that the properties of the plasma wave are mostly determined by laser intensity and plasma density. Electron acceleration by the plasma waves is discussed along with the concept of dephasing, which is another important aspect of the physics that can limit the acceleration length in an LPA. Then, methods of e-beam production will be discussed.

Section 2.5 describes the laser-plasma interaction in the context of energy transfer from the laser to electrons via the plasma medium. Scaling laws of electron energy gain in a single LPA module are discussed, which are limited by laser energy depletion if laser diffraction and electron dephasing are controlled. This laser energy depletion, also referred to as pump depletion, would not be a problem if the laser energy can be replenished. A staged LPA design has been proposed as a way to supply fresh laser pulses into the acceleration chain. Consequently, the staging of LPA modules will accelerate electrons to higher energy. Section 2.6 summarizes the concepts introduced in this chapter.

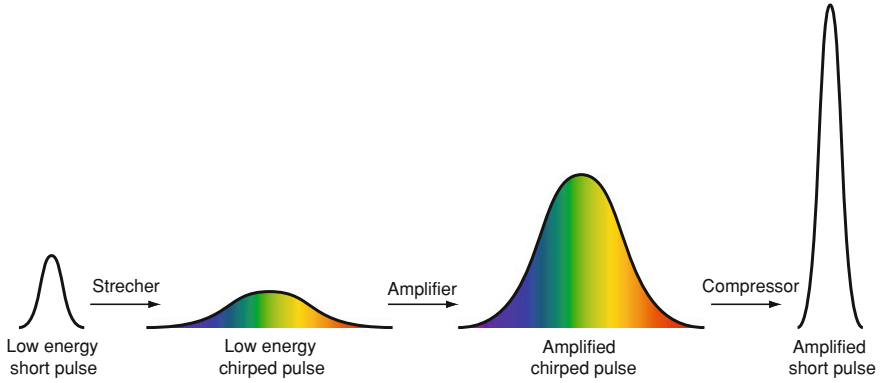


Fig. 2.1 A chirped pulse amplification system. A short, Fourier-limited laser pulse undergoes stretching, amplification, and compression. The damage in the gain medium is avoided by temporarily stretching the laser pulse and reducing the intensity. The result of the CPA system is a high energy short laser pulse. When this pulse is spatially focused, an intensity of 10^{18} to 10^{20} W/cm² is achieved

2.2 Generation of Intense Laser Pulses

2.2.1 Chirped Pulse Amplification

Chirped pulse amplification (CPA) was the breakthrough technology that expanded the realm of experimental investigation of LPAs. Excitation of plasma waves rely on intense drive laser pulses above $>10^{18}$ W/cm² and duration $\tau \leq 100$ fs. A schematic of a typical CPA laser system is shown in Fig. 2.1 [14]. Initially, the relative phase of each frequency component is zero and produces a short pulse (5–10 fs). Prior to amplification, the pulse is temporarily stretched by the dispersion in the stretcher where the different frequencies take different path lengths. The resulting pulse is a long pulse (a few hundred pico-seconds) with linearly varying instantaneous frequency with time (color gradient in the figure). This linearly varying frequency is referred to as the chirp and the frequency is described by $\omega(t) = \omega_0 + \alpha t$ where α is the chirp rate. When $\alpha > 0$ (or $\alpha < 0$), the pulsed is said to be positively (or negatively) chirped. The stretched pulse has a low intensity compared to the damage threshold of the gain medium and can be amplified. The lasing medium used in most short pulse lasers for LPA research is typically sapphire crystals doped with titanium ions (Ti:Al₂O₃), pumped with green lasers of $\lambda \sim 532$ nm to set up the population inversion in the medium. When the seed laser (the stretched laser pulse) propagates through the lasing medium, the spontaneous emission of the excited atoms amplifies the pulse. Then, the amplified long pulse propagates through a compressor which reverses the dispersion in the stretcher. As a result, a short (a few tens of femto-seconds), high intensity pulse is produced. Peak power ranging from tera-watts to recently peta-watts can be generated enabling LPA experiments [30]. When the laser

pulse is focused spatially by a focusing optic to 5–50 μm , intensity near the focus is on the order of 10^{18} to 10^{20} W/cm^2 . These intense laser pulses are necessary in LPA experiments to excite plasma waves.

The compressor in the CPA system is often used to adjust pulse duration in LPA experiments. Changing the duration is a way to change laser intensity for a given energy. The shortest duration is determined by the spectral bandwidth of the laser. Since the concept of laser pulse duration and spectral width will be used in the analysis of some of the results presented in this thesis, the mathematical framework is presented below. The temporal profile of the complex laser field can be described with $U(t) = |A(t)| \exp(i\omega_0 t + i\phi(t))$ where $|A(t)|$ is the amplitude, ω_0 is the angular frequency and $\phi(t)$ is the phase. The instantaneous frequency of the laser pulse is ,

$$\omega(t) = \omega_0 + \frac{d\phi}{dt}. \quad (2.1)$$

This is related to the frequency domain via the Fourier transform with $\omega = 2\pi\nu$,

$$V(\nu) = \int U(t) \exp(-i2\pi\nu t) dt \quad (2.2)$$

$$= |V(\nu)| \exp(i\psi(\nu)). \quad (2.3)$$

The optical intensity is $I(t) = |U(t)|^2$ and spectral intensity is $S(\nu) = |V(\nu)|^2$. They are often described with the Gaussian distributions,

$$I(t) = I_0 \exp(-2t^2/\tau^2) \quad (2.4)$$

where I_0 is the peak intensity and the pulse duration is characterized by τ . Because of the Fourier transform relation between $U(t)$ and $V(t)$, the temporal width is inversely proportional to the spectral width, and related by $\tau = \sqrt{2 \ln 2} / \pi \Delta\nu$, where $\Delta\nu$ is the bandwidth at full width half maximum (FWHM). Therefore, for a transform limited pulse (pulse without a chirp), the shortest pulse duration is set by the bandwidth of the laser pulse. When there are higher order terms in the phase, the pulse can be chirped and the intensity profile can deviate from a Gaussian distribution. By adjusting the grating spacing in the compressor, laser pulse duration, chirp and shape can be altered, and different physics can be investigated in LPA experiments.

2.2.2 TREX Laser System

The laser system used in this thesis experiment is a 40 TW CPA based laser called TREX at the LOASIS facility, LBNL. The layout of the TREX laser system is shown in Fig. 2.2. The laser pulses generated in the oscillator are amplified through five amplifying stages. Before the final amplification at the Main amplifier, the pulses are ~ 250 ps long, ~ 50 mJ/pulse. After the main amplifier, the energy of the

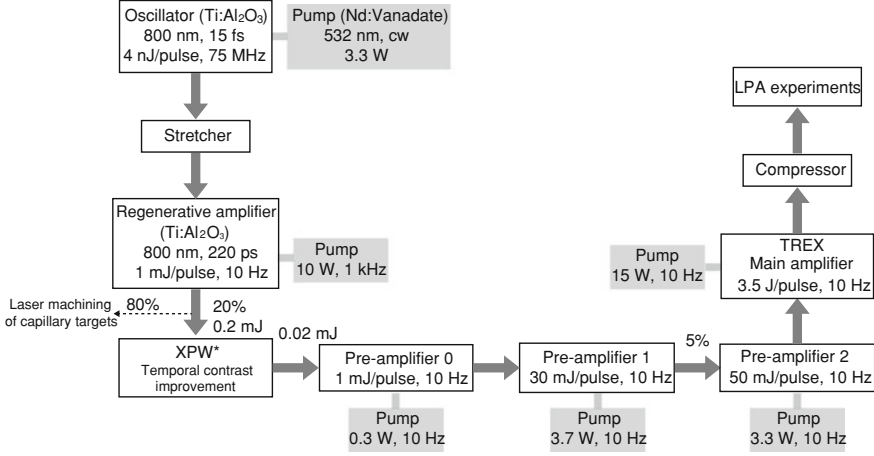


Fig. 2.2 Layout of TREX laser system at the LOASIS facility. Laser pulse duration, energy, and repetition rates are indicated. *Cross-polarized wave (XPW) system enhances temporal contrast of laser pulses [31]

laser is $\sim 3.5 \text{ J/pulse}$, of which $\sim 1.7 \text{ J/pulse}$ is transported to LPA experiments. A cross-polarized wave system, labelled as XPW, enhances temporal contrast (intensity ratio between the pulse peak and the background) of laser pulses through wave generation in a nonlinear crystal [31]. A high contrast ratio of $\sim 10^8$ to 10^9 is critical in LPA experiments, especially when the pedestal of the laser pulse is expected to ionize gas. To minimize focus shift due to thermal lensing, the TREX main amplifier is cryogenically cooled. The pulses are temporally compressed to $\sim 40 \text{ fs}$ and spatially focused to $\sim 20 \mu\text{m}$ to achieve the peak intensity of $\sim 10^{18} \text{ W/cm}^2$. In the staging experiment, each laser pulse is split into two pulses to drive the two stages. Details of the experiments will be discussed in Chap. 3.

2.3 Theory of Laser Propagation

2.3.1 Laser Diffraction

Laser diffraction imposes a limit to the energy gain in an LPA if not controlled. In this section, a mathematical formalism of laser diffraction is introduced. The optical wave is represented as a complex function of the form,

$$U(\mathbf{r}, t) = U(\mathbf{r}) \exp(i\omega t). \quad (2.5)$$

The complex amplitude takes the form $U(\mathbf{r}) = A(\mathbf{r}) \exp(i\phi(\mathbf{r}))$, where $A(\mathbf{r})$ is the amplitude and $\phi(\mathbf{r})$ is the phase of the wave at a given position \mathbf{r} . This wavefunction satisfies the wave equation,

$$\nabla^2 U - \frac{1}{c_0^2} \frac{\partial^2 U}{\partial t^2} = 0. \quad (2.6)$$

An optical wave is experimentally characterized with an intensity distribution $|U(\mathbf{r}, t)|^2$ and a wavefront which is a surface of constant phase $\phi(\mathbf{r})$.

An example of a paraxial solution to the wave equation (2.6) is a Gaussian pulse and uses Rayleigh length, z_R , as the characteristic length for diffraction. The waves are considered to be paraxial when the wavefronts are normal to paraxial rays. Paraxial waves imply that the envelope of the wave varies slowly with respect to its wavelength, $\lambda = 2\pi/k$, so that the complex amplitude can be described as, $U(r, z) = A(r, z) \exp(-ikz)$, where z is the propagation distance. Then, the complex amplitude of a Gaussian pulse is represented as,

$$U(r, z) = A_0 \frac{r_0}{r_s(z)} \exp\left(-\frac{r^2}{r_s^2(z)}\right) \exp\left(-ikz - ik \frac{r^2}{2R_c(z)} + i\zeta(z)\right), \quad (2.7)$$

where $r_s(z)$ is the laser spot size at z , r_0 is the laser spot size at focus ($z = 0$), $R_c(z)$ is the radius of curvature, and $\zeta(z)$ is the Guoy phase shift [32]. These parameters are related to z_R by,

$$\begin{aligned} z_R &= \frac{\pi r_0^2}{\lambda} \\ r_s(z) &= r_0 \left[1 + (z/z_R)^2\right]^{1/2} \\ R_c(z) &= z \left[1 + (z_R/z)^2\right] \\ \zeta(z) &= \arctan \frac{z}{z_R}. \end{aligned} \quad (2.8)$$

Other paraxial solutions to the wave equation (2.6) include Laguerre-Gaussian and Hermite-Gaussian pulses and detailed descriptions of these pulses can be found elsewhere [32, 33]. In this thesis, the effects of a transverse laser profile on wake excitation in an LPA are investigated by characterizing the drive laser with a Gaussian and a higher order Laguerre-Gaussian pulse. This analysis will be presented in Chap. 6. The propagation properties of the Gaussian pulse in vacuum are determined by r_0 and λ , which define z_R . Figure 2.3 shows on-axis intensity and laser pulse radius as a function of z_R which is the distance in which the intensity decreases by half from the focus and the pulse radius increases by $\sqrt{2}$. Due to this reduction in intensity, the acceleration length in an LPA is limited to a few z_R if diffraction is not compensated.

In experiments, the laser intensity profile is described by a spot size at focus r_0 and a Strehl ratio (SR) in the Gaussian pulse framework. The radius of a Gaussian intensity distribution is defined by

$$I(r) = I_0 e^{-2r^2/r_0^2}. \quad (2.9)$$

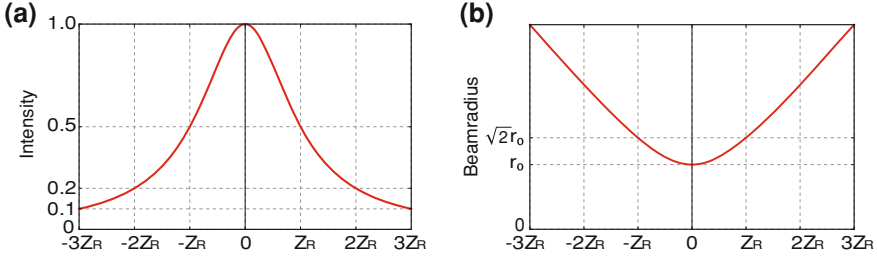


Fig. 2.3 Gaussian pulse on-axis intensity (a) and spot size (b) as a function of z_R . The graphs are normalized to the values at the focus

The SR is a measure of quality of the pulse profile compared to a Gaussian profile. It is defined as $SR = I_{\text{peak}}/I_0$, the ratio of the measured intensity peak I_{peak} to the peak intensity of the Gaussian profile I_0 . For TREX pulses used in the experiments discussed in this thesis, $r_0 \simeq 20 \mu\text{m}$, $SR \sim 0.7\text{--}0.9$, and the intensity is reduced by an order of magnitude within 5 mm ($3 z_R$).

2.3.2 Laser Guiding in Plasma Channel

Laser guiding is used to compensate for diffraction and to retain high laser intensity to extend acceleration lengths in LPAs. A plasma channel with a parabolic density profile can provide a focusing force that compensates for the diffraction of a Gaussian pulse. The mathematical formalism of a Gaussian laser propagating through a channel is as follows. Consider a parabolic plasma density profile [34, 35],

$$n(r) = n_0 + \Delta n r^2 / r_m^2, \quad (2.10)$$

where r is the radial position, n_0 is the on-axis density, and Δn is the channel depth at a matched spot size, r_m . The index of refraction for this channel is,

$$\eta_r = 1 - \frac{\omega_p^2}{2\omega_L^2} \left(1 + \frac{\Delta n r^2}{n_0 r_m^2} \right). \quad (2.11)$$

When $\Delta n = \Delta n_c = (\pi r_m^2 r_e)^{-1}$, where $r_e = e^2 / m_e c^2$ is the classical electron radius, the channel can provide guiding for a laser pulse with a Gaussian intensity profile, $|a|^2 = (a_0 r_0 / r_s)^2 \exp(-2 r^2 / r_s^2)$. In this equation, a_0 , referred to as the normalized laser vector potential, is given by

$$a_0^2 \simeq 7.3 \times 10^{-19} (\lambda [\mu\text{m}])^2 I_0 [\text{W}/\text{cm}^2]. \quad (2.12)$$

Throughout this thesis, a_0 is used to specify the strength of a laser pulse. Analysis of the paraxial equation shows that the laser evolves in the plasma channel as [5],

$$\frac{d^2 R}{dz^2} = \frac{1}{Z_M^2 R^3} \left(1 - \frac{\Delta n}{\Delta n_c} R^4 \right), \quad (2.13)$$

where $R = r_s/r_m$ and $Z_M = \pi r_m^2/\lambda$. The first term on the right-hand side of Eq. (2.13) represents vacuum diffraction and the second term represents the focusing effects of the plasma channel. The general solution to Eq. (2.13) with the initial condition $r_i = r_0$ and $dr_s/dz = 0$ (i.e. laser focused at the entrance of the plasma channel) is,

$$r_s^2 = \frac{r_i^2}{2} \left[1 + \frac{r_m^4}{r_i^4} + \left(1 - \frac{r_m^4}{r_i^4} \right) \cos \left(\frac{2\lambda z}{\pi r_m^2} \right) \right], \quad (2.14)$$

where r_i is the spot size at the entrance of channel, and z is the propagation distance [35]. Matched guiding ($r_s = r_i$) is achieved for a low power and low intensity ($a_0^2 \ll 1$) pulse when r_0 equals r_m and the laser is focused at the entrance of the channel. Here, low power is defined as the power below the critical power for the relativistic self-focusing effects, $P \ll P_c = 2c(e/r_e)^2(\omega_L/\omega_p)^2$, which will be described in detail in Sect. 2.3.3. Laser spot size evolution of matched and mismatched guiding at low intensity and low power are calculated using Eq. (2.13) and are shown in Fig. 2.4a. The entrance of the capillary is set at $z = 0$, and the plasma channel is indicated as the cyan rectangle. For matched guiding, $r_0 = r_m = 18 \mu\text{m}$, the laser retains its spot size as it propagates through the channel. For experiments

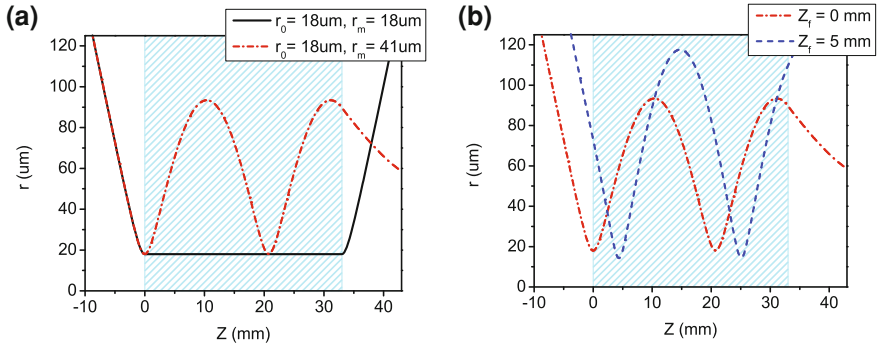


Fig. 2.4 Calculated laser spot size as a function of propagation distance in plasma channels which are indicated as shaded regions. **a** Matched guiding (solid black) for the case of $r_0 = r_m = 18 \mu\text{m}$ and mismatched guiding (dot-dashed red) for the case of $r_0 = 18 \mu\text{m}$ and $r_m = 41 \mu\text{m}$. Laser is focused at the entrance of plasma channel, $z = 0$ mm. **b** Evolution of spot sizes when pulses are focused at different locations of the same channel. Laser is focused at $z = 0$ mm (dot-dashed red) and $z = 5$ mm (dashed blue) for mismatched guiding with $r_0 = 18 \mu\text{m}$ and $r_m = 41 \mu\text{m}$

discussed in this thesis, the laser underwent mismatched guiding. One of the guiding conditions used in the experiment was $r_0 = 18 \mu\text{m}$ and $r_m = 41 \mu\text{m}$, and shown as the dot-dashed red curve. This mismatched guiding leads to a significant oscillation of the spot size. The guiding condition also changes when the laser is focused at different locations with respect to the channel entrance. Figure 2.4b shows the laser evolution for cases where the laser is focused at $z = 0 \text{ mm}$ and $z = 5 \text{ mm}$. Changing the laser focus position changes the divergence of the laser at the entrance of the channel, resulting in a different spot size evolution. Even with this intensity oscillation, the laser intensity is maintained higher than it would in a vacuum. By extending the acceleration length in an LPA using a plasma channel, e-beams were accelerated to 1 GeV in 3 cm, demonstrating an average accelerating field $>30 \text{ GV/m}$ in 2006 [15].

2.3.3 Relativistic Self-focusing

Relativistic self-focusing can focus the laser more tightly in a plasma channel than it would in a vacuum. A heuristic picture of self-focusing is introduced in this section. A more complete derivation can be found in Ref. [12]. When the laser intensity is high, the increase in the effective mass of the electrons changes the plasma frequency to $\omega_p^2 = \omega_p^2/\gamma$. This is expressed in the index of refraction by

$$\eta(r) \simeq 1 - \frac{\omega_p^2}{\omega_0^2} \frac{n_e(r)}{n_0 \gamma(r)}, \quad (2.15)$$

where ω_p is the frequency of on-axis plasma density n_0 , and $n_e(r)$ is the radial distribution of electron density, and $\gamma(r)$ is the relativistic factor associated with the transverse electron motion. Since $\gamma^2 \simeq (1 + |a|^2/2)^{1/2}$ for linearly polarized light, the index of refraction is modified as to further focus the laser to a higher a_0 .

Relativistic self-focusing allows for power and intensity dependent laser evolution in plasma channels. Self-focusing is triggered when the laser power exceeds the critical power, $P_c = 2c(e/r_e)^2(\omega_L/\omega_p)^2$. In practical units,

$$P_c[\text{GW}] \simeq 17.5 \left(\frac{\omega_L}{\omega_p} \right)^2. \quad (2.16)$$

When $P \gg P_c$, the laser spot evolution in a plasma channel [Eq. (2.13)] is modified to

$$\frac{d^2 R}{dz^2} = \frac{1}{Z_M^2 R^3} \left(1 - \frac{\Delta n}{\Delta n_c} R^4 - \frac{P}{P_c} \right). \quad (2.17)$$

Simulated spot size evolutions for low power and high power are shown in Fig. 2.5. The simulation framework, INF&NO, used for this study is described in Sect. 2.4 and

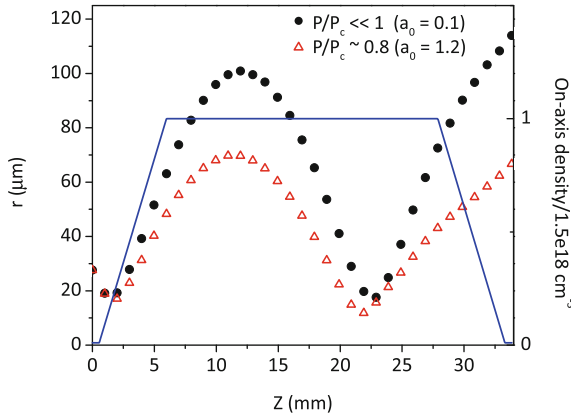


Fig. 2.5 Simulation showing the relativistic self-focusing effects in a plasma channel. Laser spot sizes r_s as a function of propagation distance for low power ($P/P_c \ll 1$) and high power ($P/P_c \simeq 0.8$) conditions used in experiments are shown. The on-axis plasma density is also shown with the blue line where $n_0 = 1.5 \times 10^{18} \text{ cm}^{-3}$

details can be found in Ref. [36]. Laser spot sizes r_s for low power ($P/P_c \ll 1$) are shown as black dots and high power ($P/P_c = 0.8$) as red triangles as a function of propagation distance. The normalized plasma density is also shown. The simulations were performed for $r_0 = 18 \mu\text{m}$, $r_m = 41 \mu\text{m}$, $n_0 = 1.5 \times 10^{18} \text{ cm}^{-3}$ and focused 1 mm into the channel as was performed in an experiment. The laser spot size for a high power laser in the channel is smaller than that for the low power laser due to self-focusing. In addition, the trailing edge of the laser pulse often exhibits stronger self-focusing than the leading edge of the pulse. This is because the index of refraction of the plasma is modified on the plasma frequency time scale and not the laser frequency time scale [5]. A detailed study of matched laser propagation in a plasma channel including the self-focusing effect is beyond the scope of this thesis and can be found elsewhere [37]. This numerical study shows that self-focusing causes power and intensity dependent laser evolution in a plasma channel, and can be used to achieve higher a_0 in plasma than in vacuum.

2.4 Plasma Waves

2.4.1 Plasma Wave Excitation

In LPAs, an underdense plasma is the medium to transfer the laser energy to accelerating electrons. Plasma is energetically the fourth state of the matter following solid, liquid, and gas in which the particles are ionized. The characteristic length of a plasma to screen a charge is known as the Debye length,

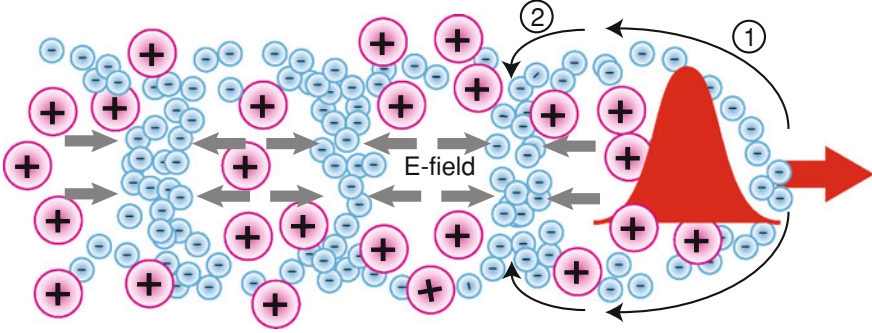


Fig. 2.6 A schematic of plasma wave excitation by an intense laser pulse. The radiation pressure of the drive laser pushes electrons out. Ions are considered to be stationary. Then, positive ions pull the electrons back, initiating electron density oscillations near the plasma frequency

$$\lambda_D = \sqrt{\frac{\epsilon_0 k_B T_e}{n_e e^2}}, \quad (2.18)$$

where ϵ_0 is the permittivity of free space, k_B the Boltzmann constant, e the electron charge, T_e the electron temperature, and n_e the electron density. Since ions move much more slowly than electrons, the ion term is neglected. For typical plasmas discussed in this thesis, $n_e \sim 10^{18} \text{ cm}^{-3}$ and $T_e \sim 10 \text{ eV}$, resulting in $\lambda_D \sim 24 \text{ nm}$. Motions less than λ_D can be neglected in the laser-plasma interaction.

Plasma waves (wakefields) are driven by the radiation pressure (also known as the ponderomotive force) of the driving laser field. A conceptual picture of wake excitation is discussed at first, and a mathematical framework will be presented afterwards. A schematic is shown in Fig. 2.6. The gradient of the laser intensity, the ponderomotive force, pushes electrons away from the propagation axis and creates a charge separation between the electrons and ions in the plasma (① in Fig. 2.6). Since the ions are much more massive than the electrons, the ions are considered stationary. After the laser pulse has passed, the restoring force described by Gauss's law initiates a local density oscillation with a characteristic plasma frequency of $\omega_p = 2\pi c/\lambda_p$ (② in Fig. 2.6). The plasma frequency is related to the background electron density, n_0 , by

$$\omega_p = \sqrt{\frac{4\pi e^2 n_0}{m_e}}, \quad (2.19)$$

where the m_e is the electron rest mass. The associated plasma wavelength in practical units is given by,

$$\lambda_p(\mu\text{m}) \cong 3.3 \times 10^{10} / \sqrt{n_0(\text{cm}^{-3})}. \quad (2.20)$$

This plasma wavelength is the characteristic scale for the accelerating structures in LPAs. For $n_0 \sim 10^{18} \text{ cm}^{-3}$, $\lambda_p \sim 33 \mu\text{m}$ and the λ_p is longer for a lower density and shorter for a higher density. The laser pulse propagates through the plasma at a group velocity, $v_g = c(1 - \omega_p^2/\omega_L^2)^{1/2}$, and continues to initiate the electro-static charge density oscillation. The phase velocity of the plasma wave roughly corresponds to the group velocity of the driving laser, $v_p \sim v_g$. This process is the excitation of a plasma wave and provides the accelerating structure to charged particles.

The amplitude of the excited field depends on plasma density n_0 and laser strength a_0 . Ionized plasmas can sustain a plasma wave with electric fields in excess of $E_0 = c m_e \omega_p / e$, where c is the speed of light in vacuum. This is known as the cold nonrelativistic wave breaking field [5]. In practical units,

$$E_0 (\text{V/m}) \cong 96 \sqrt{n_0 (\text{cm}^{-3})}. \quad (2.21)$$

This field corresponds to $\sim 96 \text{ GV/m}$ for an electron density of $n_0 \sim 10^{18} \text{ cm}^{-3}$. For example, using a linearly polarized square pulse of the optimized pulse length, the maximum excited field in the one-dimensional (1-D) limit is,

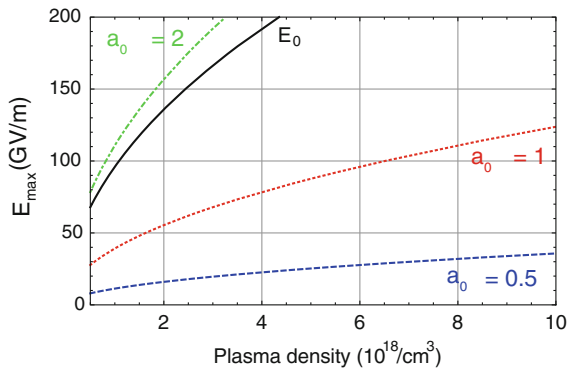
$$E_{\text{max}}(n_0, a_0) = E_0(n_0) \frac{a_0^2/2}{\sqrt{1 + a_0^2/2}}. \quad (2.22)$$

Figure 2.7 shows E_{max} for several values of a_0 as a function of n_0 . It is possible for the maximum amplitude of a nonlinear plasma wave to exceed E_0 . The nonlinear, relativistic, cold fluid wave breaking field is,

$$E_{\text{WB}} = \sqrt{2}(\gamma_p - 1)^{1/2} E_0. \quad (2.23)$$

When the field exceeds the wave breaking limit, the velocity of the background plasma electrons can exceed the phase velocity of the plasma wave and be trapped and accelerated in the plasma wave. For the parameters accessible in the experimental

Fig. 2.7 Maximum electric fields E_{max} in 1-D limit calculated using Eq. (2.22). E_0 is the cold nonrelativistic wavebreaking field defined by Eq. (2.21)



system discussed in this thesis ($n_0 \sim 1\text{--}5 \times 10^{18} \text{ cm}^{-3}$, $a_0 \sim 0.1\text{--}2$), the E_{max} ranges between 1–20 GV/m. In addition, to excite wakefields of a given amplitude at lower n_0 requires a higher a_0 laser. For example, $E_{\text{max}} \sim 80 \text{ GV/m}$ is achieved with $n_0 \sim 0.5 \times 10^{18} \text{ cm}^{-3}$ and a_0 of 2 while the same amplitude can be excited with a_0 of 1 if operated at $n_0 \sim 4 \times 10^{18} \text{ cm}^{-3}$. The balance between n_0 and a_0 influences other effects such as electron dephasing and pump depletion which will be discussed later in this chapter.

The mathematical description follows the formalism presented in Refs. [5, 38]. Introducing the vector potential \mathbf{A} and the electro-static potential Φ , the electric and magnetic fields can be expressed as $\mathbf{E} = -\nabla\Phi - \partial\mathbf{A}/\partial ct$ and $\mathbf{B} = \nabla \times \mathbf{A}$. In the Coulomb gauge ($\nabla \cdot \mathbf{A} = 0$), \mathbf{A} describes the laser and the Φ describes the plasma wave. The potentials are generally normalized as $|\mathbf{a}| = e|\mathbf{A}|/m_e c^2$ and $\phi = e\Phi/m_e c^2$. For a given laser pulse, the amplitude of the laser vector potential a_0 as defined in Eq. (2.12) is related to the transverse laser electric field by $E_L [\text{TVm}^{-1}] = 3.2 a_0 / \lambda [\mu\text{m}]$.

The excited plasma wave can be described by the density distribution n , the electric field E_z , or the potential ϕ . These values are related through $\mathbf{E} = -\nabla\phi$ and Gauss's law, $\nabla \cdot \mathbf{E} = -4\pi e(n - n_0)$. The wave equation for the density perturbation by the ponderomotive force is,

$$\left(\frac{\partial^2}{\partial t^2} + \omega_p^2 \right) \frac{\delta n}{n_0} = c^2 \nabla^2 \frac{a^2}{2}, \quad (2.24)$$

where $\delta n/n_0 = (n - n_0)/n_0$ and $\mathbf{F}_p \propto c^2 \nabla(a^2/2)$ is the ponderomotive force. A solution to the wave equation in the linear regime ($a \ll 1$) is,

$$\delta n/n_0 = (c^2/\omega_p) \int_0^t dt' \sin[\omega_p(t - t')] \nabla^2 a^2(\mathbf{r}, t')/2. \quad (2.25)$$

The sinusoidal form illustrates that the wakefield excitation is most efficient when the laser envelope length characterizing the extent of a^2 is on the order of λ_p .

In order to understand the wake excitation in the nonlinear regime ($a \gg 1$), a 1-D limit (a large transverse laser spot size) is considered. Assuming the laser pulse is slowly evolving and the phase velocity of the wave is near the speed of light, $\gamma_p^2 \gg 1$ where $\gamma_p = (1 - v_p^2/c^2)^{-1/2}$, the wake potential can be described by [10],

$$k_p^{-2} \frac{\partial^2 \phi}{\partial \xi^2} = \frac{(1 + a^2)}{2(1 + \phi)^2} - \frac{1}{2}. \quad (2.26)$$

This equation is valid in general for all a . Linear and nonlinear plasma densities and electric fields excited by laser pulses with a half-sine intensity profile are shown in Fig. 2.8. A linear regime plasma wave ($a_0 = 0.2$) is shown in Fig. 2.8a and a nonlinear regime plasma wave ($a_0 = 2$) is shown in (b). In the linear regime, the plasma wave is sinusoidal and the plasma wavelength is expressed by Eq. (2.20). In the nonlinear

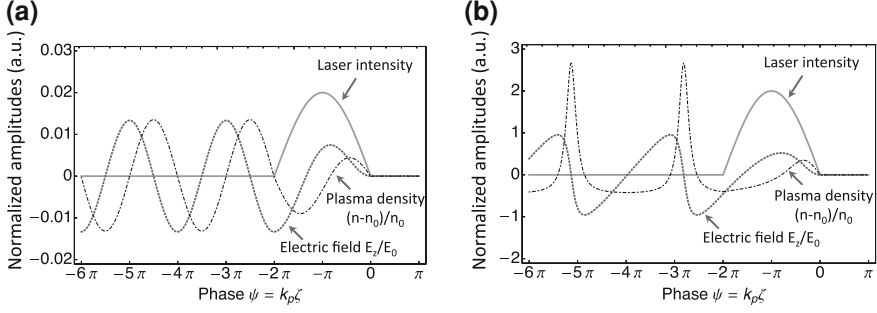


Fig. 2.8 Plasma waves and electric fields excited by laser pulses of half-sine intensities in 1-D limit. The wake potential is calculated by Eq. (2.26). **a** Linear regime where $a_0 = 0.2$. **b** Nonlinear regime where $a_0 = 2$

regime, the density profile steepens and the electric field becomes a sawtooth shape. The plasma wavelength in the nonlinear regime λ_{NP} is larger than that in the linear regime and depends on the wake amplitude:

$$\lambda_{NP} = \lambda_p \begin{cases} 1, & \text{for } E_{\max}/E_0 \ll 1 \\ (2/\pi) E_{\max}/E_0, & \text{for } E_{\max}/E_0 \gg 1. \end{cases} \quad (2.27)$$

This 1-D illustrations show the different plasma wave shapes and wavelengths between linear and nonlinear regimes.

Numerical investigations are required to understand both transverse and longitudinal electric fields in three-dimensions (3-D). Simulations using the INF&NO framework were used to demonstrate wake excitation in linear and nonlinear regimes. INF&NO is a two-dimensional cylindrical ($r - z$) particle-in-cell (PIC) code that adopts an envelope model for the laser pulse [36]. Laser-plasma interactions are described using the ponderomotive-force approximation [5]. Figure 2.9 shows simulated plasma density, E_z and E_r in linear and nonlinear regimes. Normalized plasma density distribution in a linear regime with $a_0 \sim 0.5$ and $n_0 = 1.5 \times 10^{18} \text{ cm}^{-3}$ is shown in Fig. 2.9a. In the linear regime, accelerating and decelerating fields are symmetric in size and shape as shown in Fig. 2.9b. Similarly, transverse focusing and defocusing fields are symmetric as shown in Fig. 2.9c. As a result, there is approximately $\lambda_p/4$ phase region where electrons can be both accelerated and focused as indicated with dashed red lines. In the nonlinear regime, the laser pulse almost completely blows out the plasma electrons near the back of the pulse as shown in Fig. 2.9d for $a_0 \sim 2$ and $n_0 = 1.5 \times 10^{18} \text{ cm}^{-3}$. The high electron density region outlines a shape of a bubble. This region is also called the bubble or blowout regime. The accelerating and focusing regions for electrons (bounded by dashed red lines) are larger than those in the linear regime Fig. 2.9e and f. However, for positively charged particles, the focusing region is much smaller in the nonlinear regime than in the linear regime. These simulations illustrate the difference in longitudinal and transverse wakefield profiles in linear versus nonlinear regimes.

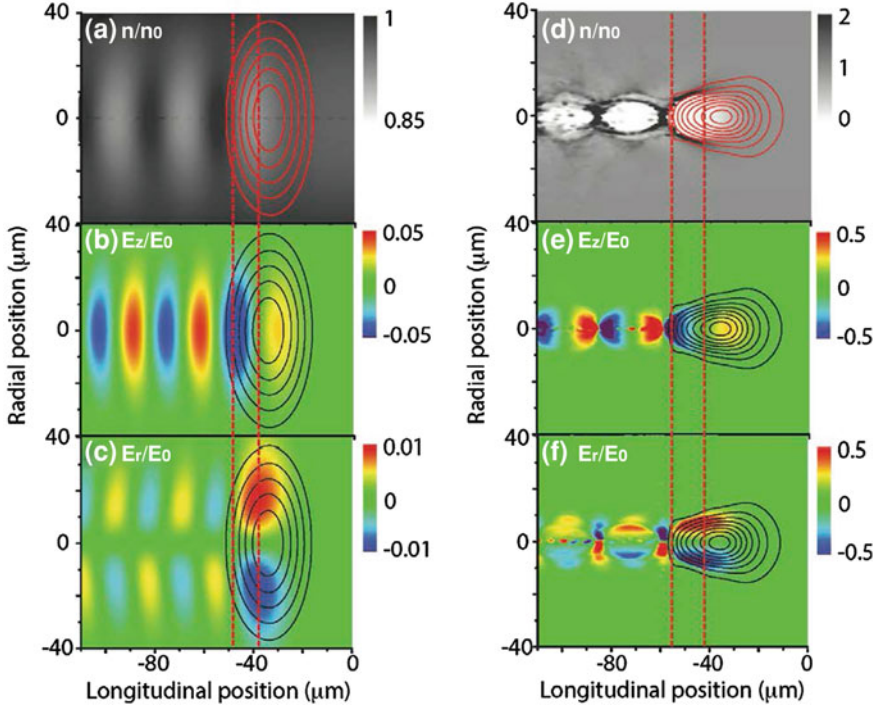


Fig. 2.9 PIC simulations of plasma wave excitations in linear (a–c) and nonlinear (d–f) regimes. The $a_0 \sim 0.5$ for the linear regime and $a_0 \sim 2$ for the nonlinear regime with $n_0 = 1.5 \times 10^{18} \text{ cm}^{-3}$. The laser intensity contours are indicated with *solid lines*. The *red dotted lines* indicate accelerating and focusing regions for electrons. The plasma density is normalized to n_0 and electric fields are normalized to $E_0 = 117 \text{ GV/m}$

In LPAs, the magnitudes of the transverse forces can also be extremely large, on the order of GV/m, requiring solid understanding and control for successful electron acceleration. In the linear to quasi-linear regime ($a_0 \lesssim 1$), the electric fields of the wake are proportional to the intensity profile. The longitudinal field is $E_z \sim \partial a^2 / \partial z$ and the transverse field is $E_\perp \sim \nabla_\perp a^2$. Therefore, the focusing force can be manipulated by tailoring the transverse laser intensity profile. Section 6.2 will present an effort to study wakefield profiles excited by different transverse laser intensity profiles. In the blowout regime ($a_0^2 \gg 1$), the focusing field can be approximately the same order of magnitude as the accelerating field, $E_z/E_0 \sim k_p \zeta / 2$ and $(E_r - B_\theta)/E_0 = (k_p r / 2)$ where E_r is the radial electric field and B_θ is the azimuthal magnetic field [5, 39–41]. This can be observed in simulated E_r/E_0 shown in Fig. 2.9f, which are roughly the same magnitudes as E_z/E_0 shown in Fig. 2.9e. At the edge of an e-beam with the spot size σ_r , the field magnitude is estimated as

$$E_r(\text{GV/m}) \simeq 9 \times 10^{-18} n_0(\text{cm}^{-3}) \sigma_r(\mu\text{m}). \quad (2.28)$$

For an LPA with $n_0 \sim 10^{18} \text{ cm}^{-3}$ and $\sigma_r \sim 0.1 \text{ } \mu\text{m}$, $E_r \sim 1 \text{ GV/m}$. Such a large focusing force implies the necessity of extremely precise control over the forces the electrons experience.

In summary, the basic physics of wake excitation by an intense laser pulse was introduced. In the linear regime ($a_0^2 \ll 1$), the plasma wave is sinusoidal and of the length $\lambda_p \propto n_0^{-1/2}$. In the nonlinear regime ($a_0^2 \gg 1$), the plasma wave steepens and the plasma wavelength increases. The amplitude of the maximum accelerating field, E_{max} , is a function of plasma density, laser strength and oscillations of focus spot size in waveguides. Large transverse forces require precise control over the electric fields and accelerating electrons in LPAs.

2.4.2 Electron Acceleration and Dephasing

In 1-D limit, electron trapping, acceleration, and dephasing can be studied by considering electron momentum and phase with respect to the plasma wave. The motion of an electron is described by a constant Hamiltonian [5],

$$H(\gamma, \psi) = \gamma(1 - \beta \beta_p) - \phi(\psi). \quad (2.29)$$

Figure 2.10 shows the electron trajectory in momentum-phase space for a constant Hamiltonian. Here, we consider a sinusoidal plasma wave, $\phi(\psi) = \phi_0 \cos(\psi)$, where $\phi_0 = 0.01$ and the phase velocity of the plasma wave $\gamma_p = 20$, and the frame is moving at the phase velocity. Trajectories of background electrons are indicated as

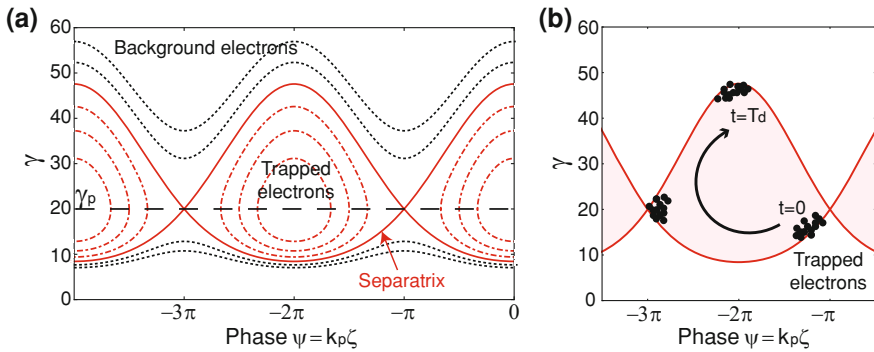


Fig. 2.10 Electron trajectory in momentum-phase space for a constant Hamiltonian. A sinusoidal plasma wave with $\gamma_p = 20$ and $\phi_0 = 0.01$ was used. **a** Trajectories of background electrons that have too much or too little momentum are shown as black dotted curves. These electrons are not trapped in the plasma waves. Trajectories of trapped electrons are shown as red curves. **b** Acceleration of trapped electrons illustrated in the momentum-phase space. Initially low energy electrons $t = 0$ outruns the plasma wave at time $t = T_d$

dotted black curves. Electrons on these trajectories have either too much or too little initial momentum, so they slip out of the plasma waves. These electrons experience accelerating and decelerating fields, but they will not be trapped in the wake. If an electron has enough initial momentum to keep up with the wake, the electron can be trapped in the plasma wave. The solid red curves indicate the momentum-phase trajectory of a trapped electron, $H = H(\gamma_p, \psi_T)$. This trajectory is referred to as the separatrix.

When the accelerating electrons gain enough energy, they will become relativistic and outrun the plasma wave. Figure 2.10b illustrates the acceleration of trapped electrons from $t = 0$ to $t = T_d$. The electrons at $t = T_d$ are now traveling at or greater than the phase velocity of the plasma wave and can no longer gain energy. This is referred to as dephasing, and is one of the limitations to the electron energy gain in LPAs. The characteristic distance of the dephasing length L_d is defined by the distance in which a highly relativistic electron phase slips by $\lambda_p/4$, roughly the phase region that is both focusing and accelerating. The dephasing lengths in linear and nonlinear regimes are given by [5],

$$L_d \simeq \frac{\lambda_p^3}{2\lambda^2} \times \begin{cases} 1, & \text{for } a_0^2 \ll 1 \\ (\sqrt{2}/\pi)a_0/N_p, & \text{for } a_0^2 \gg 1, \end{cases} \quad (2.30)$$

where N_p is the number of plasma periods behind the laser pulse. The $1/N_p$ dependence in the nonlinear regime is from the plasma wave period increasing as the laser pulse steepens, which is the dominant effect in determining the plasma wave phase velocity. Consequently, the electron beam outruns the plasma wave faster (i.e. shorter L_d). For $n_0 \sim 10^{18} \text{ cm}^{-3}$, $L_d \simeq 25\text{--}30 \text{ mm}$ for $a_0 < 2$. This length is the motivation behind using 33 mm plasma channels in experiments discussed in this thesis.

Dephasing can be mitigated by operating at lower n_0 and/or appropriately tailoring the plasma density. Since $\lambda_p \propto n_0^{-1/2}$, the accelerating electron can be kept at a fixed phase if λ_p changes to compensate for the phase slippage of the electrons due to acceleration. This can be achieved if the plasma density is increased with propagation distance, decreasing the plasma wavelength. More detailed theory on density tapering to compensate for the dephasing can be found elsewhere [29, 42, 43]. Since dephasing is another limitation to the acceleration length in LPAs following laser diffraction, its control is critical and future experimental investigations of the dephasing will be valuable.

2.4.3 Electron Beam Production

Controlled injection of electrons in a plasma wave is an active area of research in the LPA community. Recent progress includes experimental demonstration of controlled injection based on techniques using colliding pulses, ionization, and negative density gradients [20, 23, 24, 44, 45]. In this section, electron injection mechanisms using

self-trapping, ionization of nitrogen atoms, and negative plasma density gradients will be discussed. All of these injection mechanisms were demonstrated using the TREX laser system and the results will be presented in Chap. 4.

2.4.3.1 Injection Through Self-trapping

Self-trapping refers to the e-beam injection and trapping of background plasma electrons by exciting large amplitude plasma waves. Electron beam generation via self-trapping in a capillary waveguide is experimentally more straightforward than other methods, but requires high a_0 to excite the large amplitude waves. The self-trapping mechanism is explained at first in 1-D limit to illustrate the concept. The adaptation to 3-D will be qualitatively described afterwards.

In the 1-D limit, background electrons are injected when the excited wake amplitude exceeds the wave breaking field. The wave breaking field E_{WB} is the maximum electric field the plasma can sustain. In the cold fluid model, the limit is characterized as the field if all electrons were oscillating at ω_p , and is expressed in Eq. (2.21). Where the plasma wave is travelling at a large phase velocity, v_p , the plasma can sustain $E_{WB} > E_0$ where E_{WB} was introduced in Eq. (2.23). In other words, the electrons are injected if the longitudinal velocity of electrons exceeds the phase velocity of the plasma wave. Figure 2.11a is the schematic of self-trapping in 1-D and Fig. 2.10a is the electron momentum-phase space trajectory, indicating background and trapped electron trajectories. When the wake amplitude increases, the momentum of background plasma electrons increases. When the electron momentum is sufficiently large, the electrons can enter the trapped separatrix.

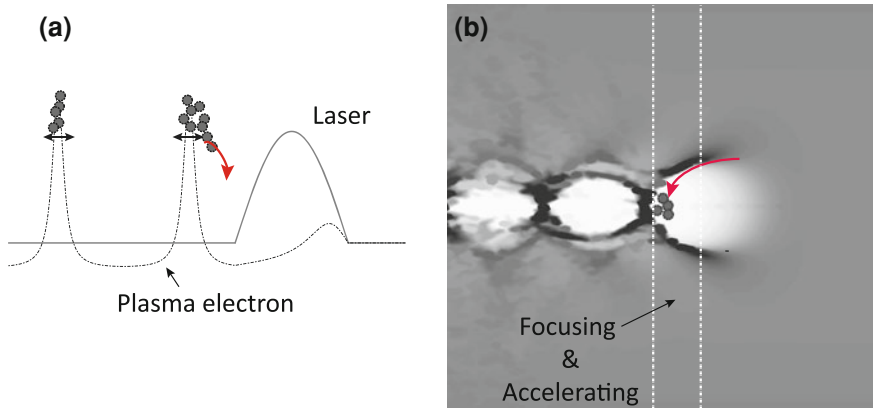


Fig. 2.11 Schematic of self-trapping of background plasma electrons in nonlinear plasma waves. **a** One-dimensional limit where background electrons are always injected via wave breaking. **b** In 3-D, laser expels all electrons behind the laser pulse in nonlinear regime. Some electrons traveling along the cavity wall, experience focusing and accelerating forces which place the electrons at the back of the bubble to be trapped

In 3-D, self-trapping is not always the longitudinal wave breaking phenomena [46]. As shown in Fig. 2.11b, increasing the laser intensity leads to a transition from sinusoidal waves to a bubble regime where all the electrons are pushed aside transversely and forms a cavity of plasma electrons. When the transverse momentum of the background electrons becomes high enough due to the ponderomotive force of the laser, the electrons can trace the wall of the plasma cavity (red arrow in the figure), experience the focusing force, and fall into the accelerating bucket. This mechanism can also lead to trapping of background electrons.

Thermal effects can lower this self-trapping threshold to below the wave breaking limit [5]. Background electron temperature is $T_e \approx 5\text{--}10\text{ eV}$ for the plasma discussed in this thesis [47]. Due to the nonzero temperature of the plasma, the electrons have a momentum spread before the wake excitation. When the plasma wave is excited, the temperature of the electrons increases in the high density regions, $T_e \propto (n/n_0)^2$ [48]. The momentum of electrons at the density peaks of the plasma wave are further increased. This increase in electron temperature can trigger self-trapping before the wavebreaking limit.

Properties of e-beams depend on parameters such as laser evolution, beam loading and dephasing [8, 15]. Self-trapped monoenergetic e-beams with a few percent energy spread were demonstrated in 2004 by three groups [6–8]. Simulations suggest that fields from injected electron bunches reduced the plasma wakefield and terminated the injection in these experiments. The trapped electrons were then accelerated to the dephasing lengths which reduced the energy spread. When electron injection is not terminated or acceleration length is not optimized for dephasing, a broad energy spread e-beam can be produced. Electron bunch production via self-trapping was investigated for the staging experiment because of its simplicity in experimental setup. Experimental results will be presented in Sect. 4.2.

2.4.3.2 Injection Through Ionization of High Z Atoms

Another way to inject background electrons is to ionize deeply bound electrons from high atomic number (Z) atoms at the proper phase within the wakefield. This is referred to as ionization injection [45, 49]. When electrons are ionized near the peak of the laser field, these electrons are already inside the plasma wave and are easily trapped. This injection method lowers the threshold of laser intensity for e-beam production compared to the self-trapping injection when the high Z atoms are suitably chosen [24, 25]. A more complete analysis of the ionization injection using nitrogen atoms is discussed elsewhere [24, 25].

Ionization of an atom by the laser field is explained by two steps: Barrier suppression and tunneling ionization. Ionization via barrier suppression is realized when the laser field is large enough to remove bound electrons. The Coulomb potential of an atom is modified by the quasi-static laser field, $V(x) = -Ze/|x| - E_x x$ [50–52]. The first term is the Coulomb potential and the second term is the modification due to the laser field. A strong laser field above $E_L = U_i^2/(4eZ)$ where U_i is the ionization potential and Z is the charge state, lowers the potential below the ionization potential,

Table 2.1 Ionization potential, corresponding intensity and a_0 for hydrogen, helium and nitrogen atoms are listed

Gas	Charge state, Z	Ionization potential (eV)	Intensity (W/cm^2)	a_0
H	1	13.6	1.4×10^{14}	0.008
He	1	24.6	1.5×10^{15}	0.03
	2	54.4	8.8×10^{15}	0.06
N	1	14.5	1.8×10^{14}	0.009
	2	29.6	7.7×10^{14}	0.02
	3	47.5	2.3×10^{15}	0.03
	4	77.4	9.0×10^{15}	0.06
	5	97.9	1.5×10^{16}	0.08
	6	552.1	1.0×10^{19}	2.2
	7	667.1	1.6×10^{19}	2.7

To calculate a_0 , $\lambda = 0.8 \mu\text{m}$ was assumed. Laser pulses of $\sim 10^{18} \text{ W}/\text{cm}^2$ will ionize H, He and the first five states of N atoms at the very leading edge of the pulse [53]

allowing the atomic electron to freely escape [50]. The required laser intensity for this barrier suppression ionization is

$$I[\text{W}/\text{cm}^2] = 4 \times 10^9 (U_i^4 [\text{eV}]/Z^2). \quad (2.31)$$

In the experiments discussed in this thesis, nitrogen was used as the high Z atom and the neutral gas was balanced with helium. The ionization potential, ionization intensity and corresponding a_0 for $\lambda = 0.8 \mu\text{m}$ are listed in Table. 2.1. Since the peak intensities of laser pulses used in experiments are $\sim 10^{18} \text{ W}/\text{cm}^2$, hydrogen, helium and the first five ionization states of nitrogen are fully ionized at the leading edge of the drive pulse.

When the laser intensity is below the barrier suppression level, the ionization of an atom can occur through tunneling ionization. The probability of tunneling ionization can be calculated with the Keldysh model [51, 54, 55],

$$W(|E_L|) = 4 \left(\frac{3}{\pi} \right)^{1/2} \Omega_0 \left(\frac{U_i}{U_H} \right)^{7/4} \left(\frac{E_H}{|E_L|} \right)^{1/2} \exp \left(-\frac{2}{3} \left(\frac{U_i}{U_H} \right)^{3/2} \frac{E_H}{|E_L|} \right), \quad (2.32)$$

where $\Omega_0 = 4 \times 10^{16} \text{ s}^{-1}$ is the characteristic atomic frequency, $U_H = 13.6 \text{ eV}$ is the ionization energy of hydrogen, and $E_H = 5.2 \text{ GV}/\text{cm}$ is the ionization field of hydrogen, and E_L is the laser field.

Unlike the outer five electrons of nitrogen atoms that are ionized at the leading edge of the laser pulse, the inner sixth and seventh electrons are ionized near the peak of the laser field. Figure 2.12 shows the ionization probability for $\text{N}^{5+} \rightarrow \text{N}^{6+}$ calculated using Eq. (2.32). The black line is with $a_0 = 1.7$ and the blue dashed line

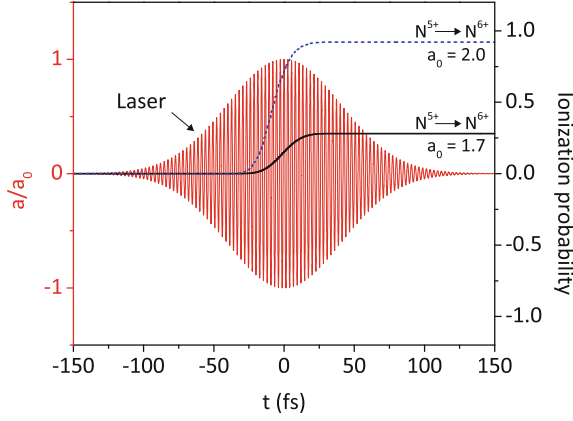


Fig. 2.12 Ionization probability for $N^{5+} \rightarrow N^{6+}$ and normalized laser vector potential, a/a_0 , versus time within the laser pulse. The *black line* is for $a_0 = 1.7$ and the *blue dashed line* is for $a_0 = 2.0$. The laser $a_0 \sim 1.5\text{--}2.0$ is the threshold of ionization injection

is with $a_0 = 2.0$. The ionization probability is $< 30\%$ for $a_0 = 1.7$ and increases to $\sim 90\%$ for $a_0 = 2.0$. This illustrates that the sixth electron is only ionized near the peak of the laser pulse and $a_0 = 1.5\text{--}2.0$ is approximately the threshold of ionization injection using nitrogen atoms. When the laser focusing is assisted by effects such as relativistic self-focusing and pulse compression, the ionization injection can be facilitated. Suitability of this method to produce e-beams in the 1st module of the staging experiment was investigated and the results will be presented in Sect. 4.2.

2.4.3.3 Injection with Negative Density Gradient

Self-trapping injection can be facilitated by tailoring the plasma density. When a laser pulse propagates in a plasma with a negative density gradient ($dn/dz < 0$), the phase velocity at the back of the wake decreases as the laser propagates [19]. In Sect. 2.4, it was introduced that the plasma wavelength increases with decreasing density ($\lambda_p \propto n_0^{-1/2}$). Plasma wavelengths for varying plasma densities are illustrated in Fig. 2.13. When the laser pulse propagates in a region with decreasing density, the plasma wavelength increases ($\lambda_{p1} < \lambda_{p2}$ where $n_1 > n_2$). The density transition changes the location of the phase peak by $\Delta\zeta = \lambda_{p1} - \lambda_{p2}$, where $\zeta = z - ct$ is the distance behind the laser pulse. If this density transition occurs over a length L , the change in the phase velocity is $\Delta v_p \sim c \Delta\zeta/L$. As discussed earlier in this section, electron injection through self-trapping occurs when the velocity of the electrons v_e exceeds the phase velocity of the plasma wave. When the phase velocity of the back of the plasma wave is reduced, injection is facilitated [5]. This effect increases with the magnitude of the density gradient. Experimental results on this technique will also be presented in Sect. 4.2.

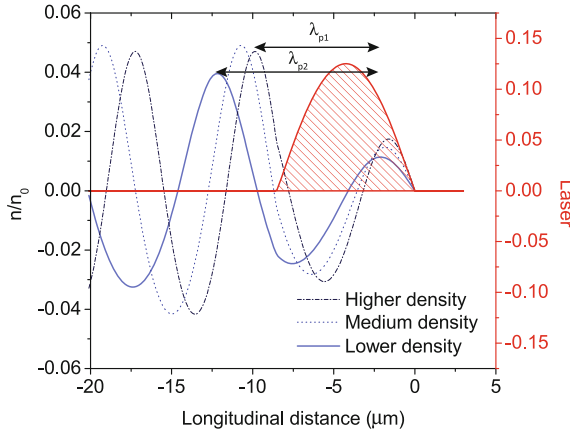


Fig. 2.13 Illustration of plasma wavelengths for three different plasma densities. When a laser propagates in a negative density gradient, phase velocity at the back of the plasma wave decreases due to the increasing λ_p and facilitates electron injection

2.5 Limitations to Energy Gain

2.5.1 Acceleration Limits

It was discussed in Chap. 1 that limitations to electron energy gain in a single LPA module are imposed by laser diffraction, electron dephasing and laser energy depletion. Laser diffraction and electron dephasing were introduced earlier in this chapter. In this section, energy depletion of the drive laser, also referred to as pump depletion will be introduced. These effects, diffraction, dephasing and depletion, limit the acceleration length and consequently possible energy gain a single stage LPA [5, 26].

As the laser excites the wakefield, the laser loses energy and eventually its intensity would be too small to further excite plasma waves. The characteristic length for the pump depletion is defined by the distance in which the laser pulse loses half of its energy to the plasma, $E_z^2 L_{pd} \simeq E_L^2 L$ where E_L is the laser field. For a linearly polarized square pulse in the 1-D limit, this length is given by [5, 56],

$$L_{pd} \simeq \frac{\lambda_p^3}{\lambda^2} \times \begin{cases} 2/a_0^2, & \text{for } a_0^2 \ll 1 \\ (\sqrt{2}/\pi)a_0, & \text{for } a_0^2 \gg 1. \end{cases} \quad (2.33)$$

For n_0 of 10^{18} cm^{-3} and a_0 of 2, L_{pd} is greater than 50 mm. The pump depletion limit on acceleration length decreases when n_0 and a_0 are large.

A summary of the characteristic lengths for diffraction, dephasing and depletion is:

- Rayleigh length: $z_R = \pi r_0^2 / \lambda$
Length in which laser diffraction reduces the intensity by half (see Sect. 2.3).
- Dephasing length:
 $L_d \simeq \lambda_p^3 / (2\lambda^2)$ for $a_0^2 \ll 1$ and $L_d \simeq (\lambda_p^3 / 2\lambda^2)(\sqrt{2}/\pi)a_0 N_p$ for $a_0^2 \gg 1$.
Lengths in which electrons outrun the plasma wave by $\lambda_p/4$ to experience accelerating and focusing forces (see Sect. 2.4).
- Depletion length:
 $L_{pd} \simeq (\lambda_p^3 / \lambda^2) 2/a_0^2$ for $a_0^2 \ll 1$ and $L_{pd} \simeq (\lambda_p^3 / \lambda^2)(\sqrt{2}/\pi)a_0$ for $a_0^2 \gg 1$.
Lengths in which the laser loses half of its energy to the plasma through wake excitation.

The laser diffraction characterized by the Rayleigh length represents the shortest acceleration limit and has to be mitigated. For experiments discussed in this thesis, r_0 was $20 \mu\text{m}$ and z_R was 1.6 mm . Diffraction was mitigated by guiding the laser in a parabolic plasma channel which was discussed in Sect. 2.3.2.

In the linear regime ($a_0^2 \ll 1$), acceleration is limited by dephasing ($L_d \ll L_{pd}$). Dephasing and depletion lengths are plotted in Fig. 2.14. For example, when $a_0 = 0.5$, $\lambda = 0.8 \mu\text{m}$, and $n_0 = 10^{18} \text{ cm}^{-3}$, the dephasing length is $L_d \sim 3 \text{ cm}$ and the pump depletion length is $L_{pd} \sim 45 \text{ cm}$. Methods to mitigate dephasing have been proposed, and experimental demonstrations are critical in the linear regime [29, 42, 43].

In the nonlinear regime ($a_0^2 \gg 1$), the dephasing length will increase and the pump depletion length will decrease, so that $L_d \sim L_{pd}$ as illustrated in Fig. 2.14. Dephasing

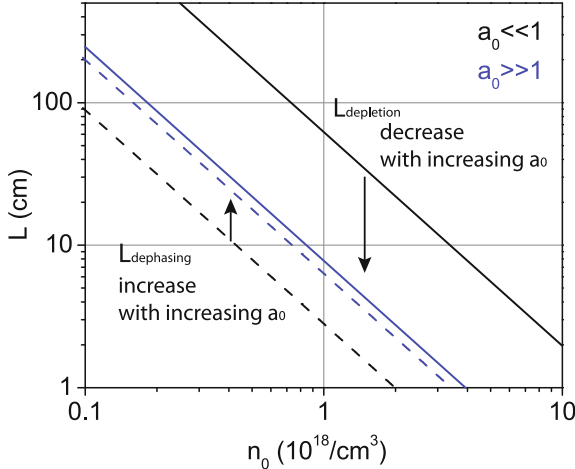


Fig. 2.14 Dephasing and depletion lengths as a function of plasma density for $a_0 \ll 1$ and $a_0 \gg 1$. For $a_0 \ll 1$, acceleration length is limited by dephasing. For $a_0 \gg 1$, both dephasing and depletion limits are similar

and depletion can be mitigated by decreasing the density since $L_d \propto n_0^{-3/2}$ and $L_{pd} \propto n_0^{-3/2}$. However, the decrease in plasma density requires a larger a_0 and a longer pulse for optimal wake excitation. In addition, the nonlinear regime also induces electron injection through self-trapping. For a dark-current free acceleration of externally injected e-beam, the nonlinear regime would not be suitable.

The quasi-linear regime characterized by $a_0^2 \sim 1$ and $L_d \sim L_{pd}$, is a favourable regime to optimize the energy gain. Laser energy is efficiently transferred to the plasma and externally injected e-beams can be accelerated without additional electron injection. Furthermore, positively charged particles can also be accelerated and focused. For these reasons, operation in the quasi-linear regime is considered to be ideal for acceleration stages in staged LPAs.

2.5.2 Scaling Laws for Energy Gain

The ideal energy gain in an LPA can be estimated by [5, 26],

$$\Delta W = eE_z L_{acc}, \quad (2.34)$$

where L_{acc} is the acceleration length and E_z is the 1-D accelerating field given in Eq.(2.22). In practical units, if the acceleration length is limited by dephasing, $L_{acc} \simeq L_d$, the energy gain is,

$$W_{dp}(\text{MeV}) \simeq \frac{630 I(\text{W/cm}^2)}{n_0(\text{cm}^{-3})} \begin{cases} 1, & \text{for } a_0^2 \ll 1 \\ (2/\pi)/N_p & \text{for } a_0^2 \gg 1. \end{cases} \quad (2.35)$$

If the L_{acc} is limited by depletion, the ideal energy gain is,

$$W_{pd}(\text{MeV}) \simeq \begin{cases} 3.4 \times 10^{21}/(\lambda^2 [\mu\text{m}^2] n_0 [\text{cm}^{-3}]), & \text{for } a_0^2 \ll 1 \\ 400 I [\text{W/cm}^2]/n_0 [\text{cm}^{-3}] & \text{for } a_0^2 \gg 1. \end{cases} \quad (2.36)$$

In the quasi-linear regime, the maximum electron energy gain using $\lambda = 0.8 \mu\text{m}$ and $n_0 = 10^{18} \text{ cm}^{-3}$ when accelerated to the depletion limit is 5 GeV. These estimates are idealized and do not consider effects such as mismatched guiding, self-focusing or other laser-plasma instabilities. For future high energy accelerators beyond energies obtainable in a single stage, the LPA design will rely on sequencing multiple stages, each driven by its own laser to supply fresh laser pulses. This coupling of LPA stages has never been demonstrated experimentally to date, and the experimental investigation of the staged LPA is the focus of this thesis.

2.6 Summary and Conclusions

This chapter provided the basic physics of LPAs. The concept of CPA laser systems, the breakthrough technology that allowed experimental investigation of LPAs, was introduced. The discussion on the production of ultraintense short laser pulses was followed by the theoretical framework of a Gaussian pulse propagation. The diffractive nature of laser pulses is a limitation to the acceleration length in the LPA if not compensated. The theory of laser guiding in a plasma channel waveguide to mitigate diffraction was discussed.

The physics of plasma wave excitation and its properties such as plasma wavelength, amplitude, and phase velocity were discussed. The properties of the plasma wave are mostly determined by laser intensity and plasma density. In the linear regime, the plasma waves are symmetric in accelerating/decelerating and focusing/defocusing fields, providing a $\lambda_p/4$ phase region for electron acceleration. In the nonlinear regime, the plasma wavelength increases and a larger phase region is suitable for electron acceleration. The concept of dephasing, which is another challenging limitation to the acceleration length in an LPA, was introduced. Then, three e-beam production methods using self-trapping, ionization of high Z atoms and negative density gradient were discussed.

Electron acceleration was then discussed in the context of energy transfer from the laser to electrons via the plasma medium. Scaling laws of electron energy gain in a single LPA module were presented. In the linear regime, the acceleration length is limited by dephasing if laser diffraction is controlled. In the nonlinear regime, dephasing and depletion lengths are similar. However, electron injection is easily triggered in the nonlinear regime, producing dark current in the LPA. The quasi-linear regime is a suitable regime for post-acceleration because the laser energy is efficiently transferred to the plasma without trapping electrons. For high energy accelerators beyond energies obtainable in a single module, the LPA design will rely on staging multiple modules to achieve desired e-beam properties and energy. This is the motivation behind the staging experiment.

Investigation of Staged Laser-Plasma Acceleration

Shiraishi, S.

2015, XVII, 121 p. 71 illus., 66 illus. in color., Hardcover

ISBN: 978-3-319-08568-5